Calculation of the long range interactions for interfacial properties

Florent Goujon, Christine Bonal, Patrice Malfreyt

Molecular Simulation
Journal of
Experimental Nanoscience

Taylor & Francis
Taylor & Francis Group

Calculation of the long range interactions for interfacial properties

Journal:	*Molecular Simulation/Journal of Experimental Nanoscience*
Manuscript ID:	GMOS-2008-0192
Journal:	Molecular Simulation
Date Submitted by the Author:	07-Oct-2008
Complete List of Authors:	Goujon, Florent; Blaise Pascal University, Chemistry Bonal, Christine; Blaise Pascal University, Chemistry MALFREYT, Patrice; Blaise Pascal University, Department of Chemistry
Keywords:	Long range corrections, Heterogeneous systems, Coulombic interactions, molecular simulations

Calculation of the long range interactions for interfacial properties.

Florent Goujon, Christine Bonal and Patrice Malfreyt[†]

[a] Laboratoire de Thermodynamique et Interactions Moléculaires,
FRE CNRS 3099, Université Blaise Pascal, 63177 Aubière Cedex, France

Abstract:
The molecular simulation of heterogeneous systems cannot be performed routinely. The results of such systems depend on the truncation procedures, size effects, long range corrections to the thermodynamic properties and on the way of calculating the Coulombic interactions. We propose here to illustrate the impact of the truncation procedures on the mechanical equilibrium of the liquid-vapor interface of alkanes. The importance of the long range corrections to the surface tension is established in alkanes, water, carbon dioxide and hydrogen sulfide liquid-vapor interfaces. The calculation of the electrostatic interactions in a slab geometry using a two-dimensional method and the standard three-dimensional Ewald summation technique is also reported.

Keywords: Heterogenous systems, molecular simulations, long range corrections, Coulombic interactions.

Submitted to Molecular Simulation for the special issue (CCP5 Special - Surfaces and Interfaces)

[†] Author to whom correspondance should be addressed.
e-mail: patrice.malfreyt@univ-bpclermont.fr

1 INTRODUCTION

Most of the phenomena in surface science (adhesion, wetting, and lubrication) involve the combination of liquid-liquid, liquid-vapour, and liquid-solid interfaces. Many important fundamental problems in chemistry and biology lead to practical applications in ion separation and extraction, drug delivery, oil recovery, and detergents. Due to the difficulties of experimental probes to access the molecular level structure of the interface, direct molecular simulation methods have become powerful techniques to examine the nature of the interface region and to calculate interfacial properties.

However, the molecular simulation of heterogeneous systems cannot be considered as routine job because the nonuniformity of the local density along the direction normal to the surface gives rise to important issues. This heterogeneity makes problems concerning the truncation procedures involved in the calculation of the force and energy equations, the long range corrections to apply to the macroscopic properties and an accurate treatment of the Coulombic interactions. Additionally, when the system is modelled by a slab geometry that is periodic in two of the three directions, the calculation of the long range Coulombic interactions cannot be applied directly.

We propose to establish the mechanical equilibrium of the liquid-vapour interface of alkanes (Figure 1a) in Monte Carlo (MC) and Molecular Dynamics (MD) simulations. This example shows the importance of the truncation procedures in the force and energy equations for heterogeneous systems. We also show that the truncation procedures can affect significantly the results of surface tensions when they are calculated using different routes. We illustrate this point by calculating the surface tension of alkanes using both a truncated force and a force modified by a cubic spline function. We complete the study of the liquid-vapour interface by showing the order of magnitude of the long range corrections to the surface tension in alkanes, water, CO_2 and H_2S systems.

In a slab geometry system where periodic boundary conditions can be used in two of the three directions, the calculation of the long range electrostatic interactions cannot be performed directly using the standard Ewald summation method. It requires to adapt the dimensions of the simulation box. We propose here to compare a two-dimensional method (HKE) [1] and the standard three-dimensional Ewald summation (EW3D,EW3DC) techniques for the calculation of the Coulombic interactions. The two-dimensional method (HKE) [1] is better adapted to systems which are periodic in two directions only but it is 20 times slower than standard three dimensional methods. The comparison between the different methods is carried out on systems constituted of monolayers of metal-chelating ligands grafted onto a graphite surface (see Figure 1b). These grafted monolayers are investigated platforms in the development of applications such as electrochemical biosensors.

2 SIMULATIONS DETAILS

2.1 Liquid-vapour interface

For the molecular simulations of the liquid-vapour interface, the total configurational energy of the systems formed by N molecules consists of intramolecular and intermolecular interactions modelled by Lennard-Jones (LJ) 6-12 sites, electrostatic point charges and a long range correction (LRC) contribution.

$$U = U_{\mathrm{INTRA}} + U_{\mathrm{INTER}} + U_{\mathrm{LRC}} \tag{1}$$

The intermolecular interactions due to the repulsion-dispersion interactions are computed using the truncated LJ potential $u_{\mathrm{LJ}}(r_{iajb})$

$$
\begin{aligned}
U_{\mathrm{LJ}} &= \sum_{i=1}^{N-1}\sum_{j>i}^{N}\sum_{a=1}^{N_i}\sum_{b=1}^{N_j} u_{\mathrm{LJ}}(r_{iajb}) \\
&= \sum_{i=1}^{N-1}\sum_{j>i}^{N}\sum_{a=1}^{N_i}\sum_{b=1}^{N_j} 4\epsilon_{ab}\left[\left(\frac{\sigma_{ab}}{r_{iajb}}\right)^{12} - \left(\frac{\sigma_{ab}}{r_{iajb}}\right)^{6}\right]
\end{aligned} \tag{2}
$$

where r_{iajb} is the distance between atom a in molecule i and atom b in molecule j, ϵ_{ab} is the energy parameter of the interaction and σ_{ab} is the Lennard-Jones core diameter. N_i is the number of atoms in the molecule i. The LJ parameters for the interactions between unlike sites are calculated by using the Lorentz-Berthelot combining rules

$$
\epsilon_{ab} = (\epsilon_{aa}\epsilon_{bb})^{1/2} \qquad\qquad \sigma_{ab} = \frac{1}{2}(\sigma_{aa} + \sigma_{bb}) \tag{3}
$$

In addition to the LJ interactions, the intermolecular interactions include the total electrostatic potential U_{ELEC} calculated using the Ewald sum method [2, 3, 4, 5] technique. For a box with orthogonal axis, U_{ELEC} is expressed as

$$
\begin{aligned}
U_{\mathrm{ELEC}} &= \frac{1}{2\epsilon_o V}\sum_{k\neq 0} Q(h)S(\mathbf{h})S(-\mathbf{h}) \\
&+ \frac{1}{8\pi\epsilon_o}\sum_{i}\sum_{a}\sum_{j\neq i} q_{ia}\sum_{b} q_{jb}\,\mathrm{erfc}\,(\alpha r_{iajb}/r_{iajb}) \\
&- \frac{\alpha}{4\pi^{3/2}\epsilon_o}\sum_{i}\sum_{a} q_{ia}^2 \\
&- \frac{1}{8\pi\epsilon_o}\sum_{i}\sum_{a}\sum_{b\neq a}\frac{q_{ia}q_{ib}}{r_{iaib}}\mathrm{erf}\,(\alpha r_{iaib})
\end{aligned} \tag{4}
$$

where $\mathrm{erfc}(x)$ is the complementary error function and $\mathrm{erf}(x)$ is the error function. α is chosen so that only pair interactions in the central cell need to be considered in evaluating the second term in Eq.(4). The functions $S(\mathbf{h})$ and $Q(h)$ are defined using Eqs.(5) and (6), respectively

$$
S(\mathbf{h}) = \sum_{i}\sum_{a} q_{ia}\exp(i\mathbf{h}.\mathbf{r_{ia}}) \tag{5}
$$

$$Q(h) = \frac{1}{h^2} \exp(-\frac{h^2}{4\alpha^2}) \tag{6}$$

where the reciprocal lattice vector $\mathbf{h}$ is defined as $\mathbf{h} = 2\pi(l/L_x, m/L_y, n/L_z)$ where l, m, n take values of $0, \pm1, \pm2, \cdots \pm\infty$. The reciprocal space sum is truncated at an ellipsoidal boundary at the vector $|\mathbf{h}^{max}|$.

As the geometry of the system shows an heterogeneity along the axis normal to the interface (z-axis), we calculate the long range correction (LRC) to the repulsion-dispersion energy as a function of z_k by splitting the cell into slabs of width δz. The total long range correction energy U_{LRC} is then calculated by summing up all of the local contributions of each slab. The long range corrections to the total energy within each kth slab are defined by two parts [6]

$$\begin{aligned} U_{\mathrm{LRC}} = \sum_{i=1}^{N_s} u_{\mathrm{lrc}}(z_k) &= \sum_{i=1}^{N_s} \left(u_{\mathrm{lrc}}^{(1)}(z_k) + u_{\mathrm{lrc}}^{(2)}(z_k) \right) \text{ with} \\ u_{\mathrm{lrc}}^{(1)}(z_k) &= \frac{8\pi}{3} \rho(z_k)^2 V_s \sum_{a=1}^{N_i} \sum_{b=1}^{N_j} \epsilon_{ab} \left[1/3 \left(\frac{\sigma_{ab}^{12}}{r_c^9} \right) - \left(\frac{\sigma_{ab}^{6}}{r_c^3} \right) \right] \qquad (7) \\ u_{\mathrm{lrc}}^{(2)}(z_k) &= \pi \rho(z_k) V_s \int_{r_c}^{\infty} dr \int_{-r}^{r} d\Delta z \sum_{i=1}^{N_s} \left[\rho(z_{k+i}) - \rho(z_{k+i-1}) \right] \; r \; U_{\mathrm{LJ,m}}(r) \qquad (8) \end{aligned}$$

where $\rho(z_k)$ and V_s are respectively the density and the volume of the slab k. Δz is defined as the difference $z - z_k$. N_s is the number of slabs between z and z_k. r_c is the cutoff radius, $U_{\mathrm{LJ,m}}(r)$ is the intermolecular energy and r the distance between the two centers of mass.

$$U_{\mathrm{LJ,m}}(r) = \sum_{a}^{N_i} \sum_{b}^{N_j} 4\epsilon_{ab} \left[\left(\frac{\sigma_{ab}}{r} \right)^{12} - \left(\frac{\sigma_{ab}}{r} \right)^{6} \right] \tag{9}$$

The first part of the long range contribution has an analytical form identical to the one associated with a homogeneous system but uses the local density $\rho(z_k)$ of the slab. The second part consists of a double integral which contains a series of density differences which render this part cumbersome to calculate.

2.2 Grafted metal-chelating monolayers onto a graphite surface

For the modelling of the grafted monolayers, we use the all-atom (AA) version of the Cornell force field AMBER [7]. The general potential function is of the form

$$\begin{aligned} U &= \sum_{bonds} k_b(r-r_o)^2 \\ &+ \sum_{angles} k_\theta(\theta-\theta_o)^2 \\ &+ \sum_{dihedrals} k_\phi[1+cos(l\phi+\delta)] \\ &+ \sum_{i=1}^{N-1}\sum_{j=i+1}^{N}\left\{4\epsilon_{ij}\left[\left(\frac{\sigma_{ij}}{r_{ij}}\right)^{12}-\left(\frac{\sigma_{ij}}{r_{ij}}\right)^{6}\right]+\sum_{l}^{\infty}{}'\frac{q_iq_j}{|\mathbf{r_{ij}}+\mathbf{n}L|}\right\} \end{aligned} \tag{10}$$

where k_b, k_θ and k_ϕ are the force constants for deformation of bonds, angles and dihedrals, respectively. The equilibrium values of bond distances and valence angles correspond to r_o and θ_o, respectively. In the dihedral angle term, l is the periodicity and δ is the phase factor. The intermolecular and intramolecular interactions consist of a van der Waals repulsion-dispersion term calculated using the Lennard-Jones (6-12) potential, represented by the penultimate term in Eq.(10). In the AMBER force field, the nonbonded interactions between atoms separated by exactly three bonds (1-4 van der Waals interactions) are reduced by a factor of 0.5 [7]. The Lennard Jones potential parameters for the interactions between unlike atoms were calculated by using the Lorentz-Berthelot mixing rules (quadratic and arithmetic rules for ϵ_{ij} and σ_{ij} parameters, respectively). The water molecules were represented with the TIP4P/2005 model [8].

When the last term in Eq.(10) is calculated with Eq.(4), the method is called EW3D and refers to the standard Ewald summation technique. When Eq.(4) is changed by the addition of $\frac{1}{2\epsilon_o V}M_z^2$, the method is called EW3DC. M_z is the net dipole moment of the simulation cell given by $\sum_{i=1}^{N} q_i\mathbf{r}_i$. This contribution is the correction term from Yeh and Berkowitz [9] which results by the plane-wise summation method proposed by Smith [3].

Adding this term to the total energy amount to using a z-component force for each atom given by

$$F_{i,z} = -\frac{q_i}{\epsilon_o V} M_z \tag{11}$$

The EW3DC method differs from the standard EW3D method only by the presence of this dipole correction. However, these two three-dimensional method require to change the primary simulation box by adding two empty spaces between the periodic image in order to dampen out the interslab interactions [9, 10, 11].

The total Coulombic interactions for a two-dimensional periodic system which is finite in the z-dimension can be calculated using the Hautman and Klein method [1]. This method is in fact an adaptation of the Ewald technique for systems which are periodic in two dimensions only. The operational expressions of the total electrostatic interactions can be found elsewhere [1] for completeness.

The computational procedures of the molecular simulation of the liquid-vapour interface can be found in previous papers [12, 13, 14, 15, 16, 17]. The force-field used in the molecular modelling of the grafted system and the description of the computational procedures can be also found elsewhere [11]. Figures 1a and 1b show typical configurations of the liquid-vapour interface of the n-pentane and of the NTA grafted system, respectively. In these snapshots, z refers to the direction of the heterogeneity.

3 RESULTS AND DISCUSSIONS

We propose here to illustrate the importance of the truncation procedures for the mechanical equilibrium of the liquid-vapour interface of alkanes. The impact of the discontinuities in the force and energy equations is also studied for the different definitions of the surface tension. The long range corrections to the surface tension are reported for systems involving both electrostatic and dispersion-repulsion energy contributions. We finish by

the calculation of the electrostatic interactions in a slab geometry system.

3.1 Calculation of the normal and tangential pressure components

In the case of a planar liquid-vapour surface lying in the x,y plane where the heterogeneity takes place along the z direction normal to the surface, the calculation of the normal and tangential pressure components along this axis is meaningful for the validation of the mechanical equilibrium. The components of the pressure tensor calculated from the Irving and Kirkwood definition [18, 19, 20] are expressed by

$$\begin{aligned} p_{\alpha\beta}(z_k) &= \langle \rho(z_k) \rangle \, k_B T \mathbf{I} \\ &+ \frac{1}{A} \left\langle \sum_{i=1}^{N-1} \sum_{j>i}^{N} (\mathbf{r}_{ij})_\alpha (\mathbf{F}_{ij})_\beta \frac{1}{|z_{ij}|} \theta\left(\frac{z_k - z_i}{z_{ij}}\right) \theta\left(\frac{z_j - z_k}{z_{ij}}\right) \right\rangle \end{aligned} \tag{12}$$

where $\mathbf{I}$ is the unit tensor and T is the input temperature. α and β represent x, y or z directions. $\theta(x)$ is the unit step function defined by $\theta(x) = 0$ when $x < 0$ and $\theta(x) = 1$ when $x \geq 0$. A is the surface area normal to the z axis. The distance z_{ij} between two molecular centers-of-mass is divided into N_s slabs of thickness δz. Following Irving and Kirkwood, the molecules i and j give a local contribution to the pressure tensor in a given slab if the line joining the centers-of-mass of molecules i and j crosses, starts or finishes in the slab. Each slab has $1/N_s$ of the total contribution from the $i-j$ interaction. The normal component $p_{\mathrm{N}}(z_k)$ is equal to $p_{\mathrm{zz}}(z_k)$ whereas the tangential component is given by $\frac{1}{2}(p_{\mathrm{xx}}(z_k) + p_{\mathrm{yy}}(z_k))$. $\mathbf{F}_{ij}$ in Eq.(12) is the intermolecular force between molecules i and j and is expressed as the sum of all the site-site forces acting between these two molecules.

$$\begin{aligned} \mathbf{F}_{ij} &= \sum_{a=1}^{N_i} \sum_{b=1}^{N_j} (\mathbf{f}_{iajb}) \\ &= -\sum_{a=1}^{N_i} \sum_{b=1}^{N_j} \frac{\mathbf{r}_{iajb}}{r_{iajb}} \frac{dU(r_{iajb})}{dr_{iajb}} \end{aligned} \tag{13}$$

For the simulation of the liquid-vapour interface of alkanes, the total intermolecular energy U is calculated by using the LJ potential U_{LJ} because no electrostatic interactions are

involved in the model. In our MC simulations, the LJ potential is truncated at the cutoff radius (r_c = 12 Å) according to U_{T}

$$U_{\mathrm{T}}(r_{iajb}) = \begin{cases} U_{\mathrm{LJ}}(r_{ij}) & r_{iajb} < r_c \\ 0 & r_{iajb} \geq r_c \end{cases} \tag{14}$$

The calculation of the pressure components requires the use of the derivative of the potential. This derivative can be calculated using either the truncated force expressed as

$$f_{\mathrm{T}}(r_{iajb}) = \begin{cases} -\dfrac{\partial U_{\mathrm{LJ}}}{\partial r_{iajb}} & r_{iajb} < r_c \\ 0 & r_{iajb} \geq r_c \end{cases} \tag{15}$$

or the truncated force modified by the addition of an impulse contribution [21] defined by

$$f_{\mathrm{TC}}(r_{iajb}) = \begin{cases} -\dfrac{\partial U_{\mathrm{LJ}}}{\partial r_{iajb}} & r_{iajb} < r_c \\ +\dfrac{U_{\mathrm{LJ}}(r_c)}{\Delta r} & r_c < r_{iajb} < r_c + \Delta r \\ 0 & r_{iajb} \geq r_c + \Delta r \end{cases} \tag{16}$$

where Δr is equal to 0.05 Å for a cutoff of 12 Å. In the most cases, the MD simulations used a truncated force and the MC simulations a truncated potential. Figure 2 shows the profiles of the normal p_{N} and tangential p_{T} components of the pressure tensor calculated from MC and MD configurations. For a planar surface, the mechanical equilibrium requires to have $p_{\mathrm{N}}(z)$ and $p_{\mathrm{T}}(z)$ constant and equal to p in the bulk phases. In the interfacial region, p_{T} exhibits two negative peaks indicating that the liquid phase is under tension. The normal and tangential components of the pressure calculated from MD are shown in Figure 2a. These profiles establish the mechanical equilibrium of these MD configurations as expected for a method that uses the forces to generate the evolution of the system. On the other hand, in MC configurations when the forces are calculated from Eq.(15), the profiles of p_{N} and p_{T} highlight that the configurations are not in mechanical equilibrium. This can be explained by the fact that MC uses the configurational energy to generate the configurations and that the pressure is calculated from the derivative of the configurational

energy. When the configurational energy is calculated with a truncated potential which is not differentiable at the cutoff radius, the truncated force used in the calculation of the pressure does not correspond to the truncated potential. To match the force and energy equations, the force must be corrected by an addition term. When the force is corrected as in Eq.(16), the profiles of the normal and tangential components of Figure 2b show that the mechanical equilibrium is satisfied within the MC configurations.

Another way of removing the discontinuities in the energy and force equations is to use the Lennard-Jones potential modified by a cubic spline. The potential and force equations become

$$U_{\mathrm{SP}}(r_{iajb}) = \begin{cases} U_{\mathrm{LJ}}(r_{iajb}) - U_{\mathrm{LJ}}(r_s) + a & r_{iajb} < r_s \\ -\frac{b}{3}(r_{iajb} - r_c)^3 - \frac{c}{4}(r_{iajb} - r_c)^4 & r_s \leq r_{iajb} < r_c \\ 0 & r_{iajb} \geq r_c \end{cases} \tag{17}$$

$$f_{\mathrm{SP}}(r_{ij}) = \begin{cases} -\dfrac{\partial U_{\mathrm{LJ}}}{\partial r_{iajb}} & r_{iajb} < r_s \\ +b(r_{iajb} - r_c)^2 + c(r_{iajb} - r_c)^3 & r_s \leq r_{iajb} < r_c \\ 0 & r_{iajb} \geq r_c \end{cases} \tag{18}$$

Using such expressions, the potential and its derivative are continuous at the cutoff. The parameters a, b and c are calculated by requiring that the first and second derivatives of the u_{SP} potential be continuous at r_s and r_c.

$$\begin{aligned} c &= +\frac{\frac{\partial^2 U_{\mathrm{LJ}}}{\partial r_{ij}^2}(r_s)}{(r_s - r_c)^2} - 2\frac{\frac{\partial U_{\mathrm{LJ}}}{\partial r_{ij}}(r_c)}{(r_s - r_c)^3} \\ b &= -\frac{\frac{\partial^2 U_{\mathrm{LJ}}}{\partial r_{ij}^2}(r_s)}{(r_s - r_c)} + 3\frac{\frac{\partial U_{\mathrm{LJ}}}{\partial r_{ij}}(r_s)}{(r_s - r_c)^2} \\ a &= -\frac{b}{3}(r_s - r_c)^3 - \frac{c}{4}(r_s - c)^4 \end{aligned} \tag{19}$$

Figures 3a and 3b display the profiles of the normal and tangential pressure components calculated over MC and MD configurations using the potential and force of Eqs. (17) and (18), respectively. The profiles match very well within the MC and MD methods and indicates the primary importance of the discontinuity of the potential at the cutoff. Additionally, the total local chemical potential calculated from Eq.(20) exhibits a flat profile as expected for a planar liquid-vapour interface at equilibrium:

$$\mu(z_k) = kT \ln \left(\left\langle \frac{\Lambda^3 \rho(z_k)}{\exp(-\Delta U / k_B T)} \right\rangle_{z_k, NVT} \right) \tag{20}$$

where Λ is the de Broglie thermal wavelength and U is the potential changed by a cubic spline function. ΔU represents the energy of the ghost $(N+1)$ particle with the N particles. The local expression of the chemical potential was established by Widom [22].

The discontinuity in the force and energy equations was not considered as crucial in the simulations of a homogeneous fluid where there was a compensation between the forces affecting a particle from outside is cutoff sphere. In the case of heterogeneous system, this assumption is not longer valid and the equivalence between MC and MD is recovered only when the discontinuities are removed. In this case, the MC and MD simulations are performed with the same potential.

3.2 Calculation of the surface tension

In the case of the calculation of the surface tension, the discontinuities in the energy and forces expressions can lead to significant differences between the different routes. Some definitions use the potential energy in their working expressions. For instance, the test-area (TA) method [23] recently developed uses the perturbation formalism to express the surface tension. Other expressions (KB [24]) and (IK [25, 19, 20]) are based upon the mechanical definition of the surface tension and use the derivative of the potential in their operational expressions. Table 1 shows that the intrinsic part of the surface tension calculated from the potential energy (TA) is different with that calculated from the derivative of the potential energy (IK,KB). However, when the discontinuities are removed in the expressions of the force and energy with a cubic spline function, the intrinsic part is identical within IK, KB and TA approaches. The equivalence between the different operational expressions can be also recovered by making the potential and force equations consistent [14].

An other important contribution to the surface tension is the long range contribution due to the fact that interactions are neglected from the cutoff region. The appropriate LRC of the normal and tangential components of the pressure tensor within the IK defintion have been derived by Guo and Lu [6] and are composed of two parts as expressed in Eqs. (21) and (22).

$$\begin{aligned} p_{\mathrm{N,LRC}}(z_k) &= p^{(1)}_{\mathrm{N,LRC}}(z_k) + p^{(2)}_{\mathrm{N,LRC}}(z_k) \\ &= -\frac{2\pi}{3}\rho^2(z_k)\int_{r_c}^{\infty} dr r^3 \ \frac{dU_{\mathrm{LJ,m}}(r)}{dr} \\ &- \ \pi\rho(z_k)\int_{r_c}^{\infty} dr \int_{-r}^{r} d\Delta z \ [\rho(z)-\rho(z_k)] \frac{dU_{\mathrm{LJ,m}}(r)}{dr} \ (\Delta z)^2 \end{aligned} \tag{21}$$

As concerns the tangential pressure, the first term is identical to the first term of the normal component whereas the second term is expressed by

$$p^{(2)}_{\mathrm{T,LRC}}(z_k) = -\frac{\pi}{2}\rho(z_k)\int_{r_c}^{\infty} dr \int_{-r}^{r} d\Delta z \ [\rho(z)-\rho(z_k)] \frac{dU_{\mathrm{LJ,m}}(r)}{dr} \ \left[r^2-(\Delta z)^2\right] \tag{22}$$

The first term of $p_{\mathrm{N,LRC}}(z_k)$ and $p_{\mathrm{T,LRC}}(z_k)$ is identical to that used in homogeneous molecular simulations by using a local density $\rho(z_k)$ instead of a scalar density ρ whereas the second term takes into account the density differences between the slabs. From these LRC expressions, it is then possible to calculate the LRC parts relative to the surface tension. From a mechanical viewpoint, the surface tension can be also calculated from the integration of the difference of the normal and tangential components of the pressure tensor [18, 19, 20] across both interfaces according to

$$\gamma = \gamma_{\mathrm{I}} + \gamma_{\mathrm{LRC}} \tag{23}$$

$$= \frac{1}{2}\int_{-L_z/2}^{+L_z/2} dz \, (p_{\mathrm{N}}(z_k) - p_{\mathrm{T}}(z_k)) + \frac{1}{2}\int_{-L_z/2}^{+L_z/2} dz \, (p_{\mathrm{N,LRC}}(z_k) - p_{\mathrm{T,LRC}}(z_k)) \tag{24}$$

where the first term is related to the intrinsic part of the surface tension and the second one corresponds to the LRC part.

Figure 4a shows the profiles of the difference between the normal and tangential components as a function of the z direction. We observe that the two profiles are well symmetric with a well established liquid bulk phase. The integral of the profile is represented on the right axis. The integral allows to check that the contributions to the surface tension are the same for the two interfaces with a flat profile between them. Figure 4b plots the profile of the long range corrections to $p_N - p_T$ difference with the integral of this property represented on the right axis. The profile of the long range corrections to the pressure components indicates that the contribution of each interface is identical and there is no contribution in the bulk phases. The total value of the long range correction to the surface tension is far from being negligible: in this case, it represents up to 30 % of the total surface tension. The calculation of the surface tension requires the use of appropriate long range corrections; each operational expression of the surface tension must be corrected by specific long range corrections. This was described in detail elsewhere [14]. Interestingly, Table 2 shows the intrinsic surface tension with its long range corrections for some alkanes, water, carbon dioxide and hydrogen sulfide. In water, the long range corrections to the surface tension are small whereas the electrostatic contribution to the surface tension is negative. In CO_2 and H_2S, the dispersion-repulsion contributions are greater than the electrostatic interactions; the long range corrections to the surface tension represents then about 30 % of the total value.

3.3 Calculation of the electrostatic interactions in a slab geometry

The calculation of the electrostatic interactions in a system represented by a slab geometry must be carefully undertaken. The use of two-dimensional method such as the Hautmann-Klein method (HKE) [1] is recommended for systems which are periodic in two dimensions only. However, the two-dimensional methods are cumbersome and time-consuming. The HKE method is about 20 times slower than the standard Ewald methods (EW3D, EW3DC). It is then fundamental from a methodological viewpoint to check that

the 2D and 3D methods lead to the same energetical, structural and electrical properties in slab geometry systems. We propose to check these points on a system formed by negatively charged monolayers of chelating copper (NTA) compounds immobilized onto a HOPG graphite surface in aqueous solution. The use of a three-dimensional method in a slab geometry system requires to elongate the simulation box in the z direction in order to dampen out the interslab interactions. Figure 5a depicts the number of hydrogen bonds between water molecules in the region close to the surface. The criteria used for the calculation of the number of hydrogen bonds can be found in a previous paper [11]. This figure demonstrates that the number of hydrogen bonds between water molecules close to the grafted surface does not depend on the method used for the calculation of the electrostatic interactions indicating that KHE, EW3D and EW3DC methods give the same structure of water. The charge density profiles of water molecules is reported in part b of Figure 5 for each method. This figure tends to establish that the distribution of charges of water molecules is slightly perturbed close to the surface. This is due to the presence of grafted molecules that are able to interact preferentially with water molecules to give hydrogen bonds. However, from 20 Å, the charge density profile recovers an expected zero value. We observe that the three methods give the same charge density profiles. The analysis of the electric field profile $E(z)$ (Figure 5c) calculated from the integral of the charge density profile confirms that the electric field reaches a constant zero from 20 Å. From this value of z, the distribution of water molecules is isotropic as expected for a bulk-like region. This indicates that the surface and the grafted molecules do not influence significantly the water molecules within this region. Additionally, the calculation of these electric properties allows to validate the use of three-dimensional methods for the calculation of the Coulombic interactions in a slab geometry.

4 Conclusions

We have shown that the use of truncated potential and truncated force may lead to significant differences in the mechanical equilibrium and surface tensions of liquid-vapour systems governed by dispersion-repulsion interactions. Removing the discontinuities in the potential and force equations amounts to recovering the equivalence between MC and MD and to making consistent the different routes of the calculation of the surface tension. Whereas the effects of these discontinuities are compensated in the simulation of bulk phases, they must be taken into account in the simulation of two-phase systems.

The simulation of slab geometry system requires to do a compromise between an accurate treatment of the Coulombic interactions, the use of fully developed system and the number of steps to obtain a good convergence of the thermodynamic and electrical properties. A solution consists in using a slight modified three-dimensional Ewald summation method with the addition of empty space between the primary simulation cell. We have compared the results between three-dimensional methods and a two-dimensional method. We have concluded that the standard Ewald summation technique can be used with confidence in such slab geometries.

References

[1] J. Hautmann and M. L. Klein, *An ewald summation method for planar surfaces and interfaces*, Mol. Phys., 75 (1992), 379.

[2] M. P. Allen and D. J. Tildesley, *Computer Simulation of Liquids*, Clarendon Press, Oxford, (1989).

[3] E. R. Smith, *Electrostatic energy in ionic crystals*, Proc. R. Soc. Lond. A., 375 (1981), 475.

[4] D. M. Heyes, *Pressure tensor of partial-charge and point-dipole lattices with bulk and surface geometries*, Phys. Rev. B, 49 (1994), 755.

[5] J. Alejandre, D. J. Tildesley, and G. A. Chapela, *Molecular dynamics simulation of the orthobaric densities and surface tension of water*, J. Chem. Phys., 102 (1995), 4574.

[6] M. Guo and B. C. Y. Lu, *Long range corrections to thermodynamic properties of inhomogeneous systems with planar interfaces*, J. Chem. Phys., 106 (1997), 3688.

[7] W. D. Cornell, P. Cieplak, C. I. Bayly, I. R. Gould, K. M. Merz, D. M. Ferguson Jr, D. M. Fox, T. Spellemer, J. W. Caldwell, and P. Kolleman, *A second generation force field for the simulation of proteins, nucleic acids, and organic molecules*, J. Am. Chem. Soc., 117 (1995), 5179.

[8] J. L. F. Abascal and C. Vega, *A general purpose model for the condensed phases of water: Tip4p/2005*, J. Chem. Phys., 123 (2005), 234505.

[9] I. C. Yeh and M. L. Berkowitz, *Ewald summation for systems with slab geometry*, J. Chem. Phys., 111 (1999), 3155.

[10] S. Crozier, R. L. Rowley, E. Spohr, and D. Henderson, *Comparison of charged sheets and corrected 3d ewald calculations of long-range forces in slab geometry electrolyte systems with solvent molecules.* J. Chem. Phys., 112 (2000), 9253.

[11] F. Goujon, C. Bonal, B. Limoges, and P. Malfreyt, *Molecular simulations of grafted metal-chelating monolayers: methodology, structure and energy*, Mol. Phys., 106 (2008), 1397.

[12] F. Goujon, P. Malfreyt, A. Boutin, and A.H. Fuchs, *Direct monte carlo simulations of the equilibrium properties of the n−pentane liquid−vapor interface*, *J. Chem. Phys.*, 116 (2002), 8106.

[13] F. Goujon, P. Malfreyt, J.M. Simon, A. Boutin, B. Rousseau, and A. H. Fuchs, *Monte carlo versus molecular dynamics simulations in heterogeneous systems: An application to the n-pentane liquid-vapor interface*, J. Chem. Phys., 121 (2004), 12559.

[14] C. Ibergay, A. Ghoufi, F. Goujon, P. Ungerer, A. Boutin, B. Rousseau, and P. Malfreyt, *Molecular simulations of the* n*-alkane liquid-vapour interface: interfacial properties and their long range corrections*, Phys. Rev. E, 75 (2007), 051602.

[15] A. Ghoufi, F. Goujon, V. Lachet, and P. Malfreyt, *Expressions for local contributions to the surface tension from the virial route*, Phys. Rev. E, 77 (2008), 031601.

[16] A. Ghoufi, F. Goujon, V. Lachet, and P. Malfreyt, *Calculation of the surface tension of acid gazes and water from monte carlo simulations*, J. Chem. Phys., 128 (2008), 154716.

[17] A. Ghoufi, F. Goujon, V. Lachet, and P. Malfreyt, *Multiple histogram reweighting method for the surface tension calculation*, J. Chem. Phys., 128 (2008), 154718.

[18] J. S. Rowlinson and B. Widom, *Molecular Theory of Capillarity.* Clarendon Press, Oxford, (1982).

[19] J. P. R. B. Walton, D. J. Tildesley, J. S. Rowlinson, and J. R. Henderson, *The pressure tensor at the planar surface of a liquid*, Mol. Phys., 48 (1983), 1357.

[20] J. P. R. B. Walton and K. E. Gubbins, *The pressure tensor in an inhomogeneous fluid of non-spherical molecules*, Mol. Phys., 58 (1986), 1013.

[21] A. Trokhymchuk and J. Alejandre, *Computer simulations of liquid/vapor interface in lennard-jones fluids: Some questions and answers*, J. Chem. Phys., 111 (1999), 8510.

[22] B. Widom, *Structure of interfaces from uniformity of the chemical potential*, J. Stat. Phys., 19 (1978), 563.

[23] G. J. Gloor, G. Jackson, F. J. Blas, and E. de Miguel, *Test-area simulation method for the direct determination of the interfacial tension of systems with continuous or discontinuous potentials*, J. Chem. Phys., 123 (2005), 134703.

[24] J. G. Kirkwood and F. P. Buff, *The statistical mechanical theory of surface tension*, J. Chem. Phys., 17 (1949), 338.

[25] J. H. Irving and J. G. Kirkwood, *The statistical mechanical theory of transport processes. iv. the equations of hydrodynamics* J. Chem. Phys., 18 (1950), 817.

Table 1: Surface tensions of methane (mN m^{-1}) calculated from MC simulations using a truncated LJ potential and a modified LJ potential using the KB, IK and TA approaches. The cutoff radius is fixed to 12 Å.

γ_{KB}	γ_{IK}	γ_{TA}
Truncated potential		
9.5	9.5	10.6
Spline potential		
8.5	8.5	8.5

Table 2: Lennard-Jones, electrostatic and long range corrections contributions to the surface tension (mN m^{-1}) calculated from MC simulations in different liquid-vapour systems.

	γ_{LJ}	γ_{ELE}	γ_{LRC}	γ_{TOT}	$\gamma_{\mathrm{EXP.}}$
CH_4	9.5		3.8	13.3	11.3
nC_5	12.0		5.6	17.6	15.3
nC_{10}	6.0		4.3	10.3	10.4
H_2O	-87.6	117.7	3.5	33.6	36.5
CO_2	6.1	2.9	2.5	11.5	12.0
H_2S	21.0	9.3	8.0	38.3	37.5

Fig. 1 a) Configurations of the n-pentane liquid-vapour interface at T = 350 K. b) Snapshot of a MD configuration of 10 grafted NTA-Cu(II) complexed onto the HOPG surface with the water molecules.

Fig. 2 a) Normal and tangential pressure components calculated in the liquid-vapour interface of the n-pentane at T = 325 K a) from MC using a truncated potential and MD using a truncated force; b) from MC using both a truncated force f_{T} and a truncated force modified by an additional impulse f_{TC}.

Fig. 3 Normal and tangential pressure components calculated in the liquid-vapour interface of the n-pentane at T = 325 K from a) MC and b) MD using a Lennard-Jones potential and a force changed by a cubic spline function. c) Total chemical potential of the liquid-vapour interface of methane at T = 120 K calculated from MC simulations using a LJ potential changed by a cubic spline function.

Fig. 4 a) Difference between the normal and tangential pressure profiles for the liquid-vapour interface of the n-pentane at T = 300 K; b) Difference between the normal and tangential components of the long range corrections to the pressure tensor. On the right axis, the integral of each difference is plotted as a function of z.

Fig. 5 a) Profiles of the number of hydrogen bonds between water molecules along the direction normal to the surfaces. b) charge density and c) electric field profiles along the direction normal to the surface.

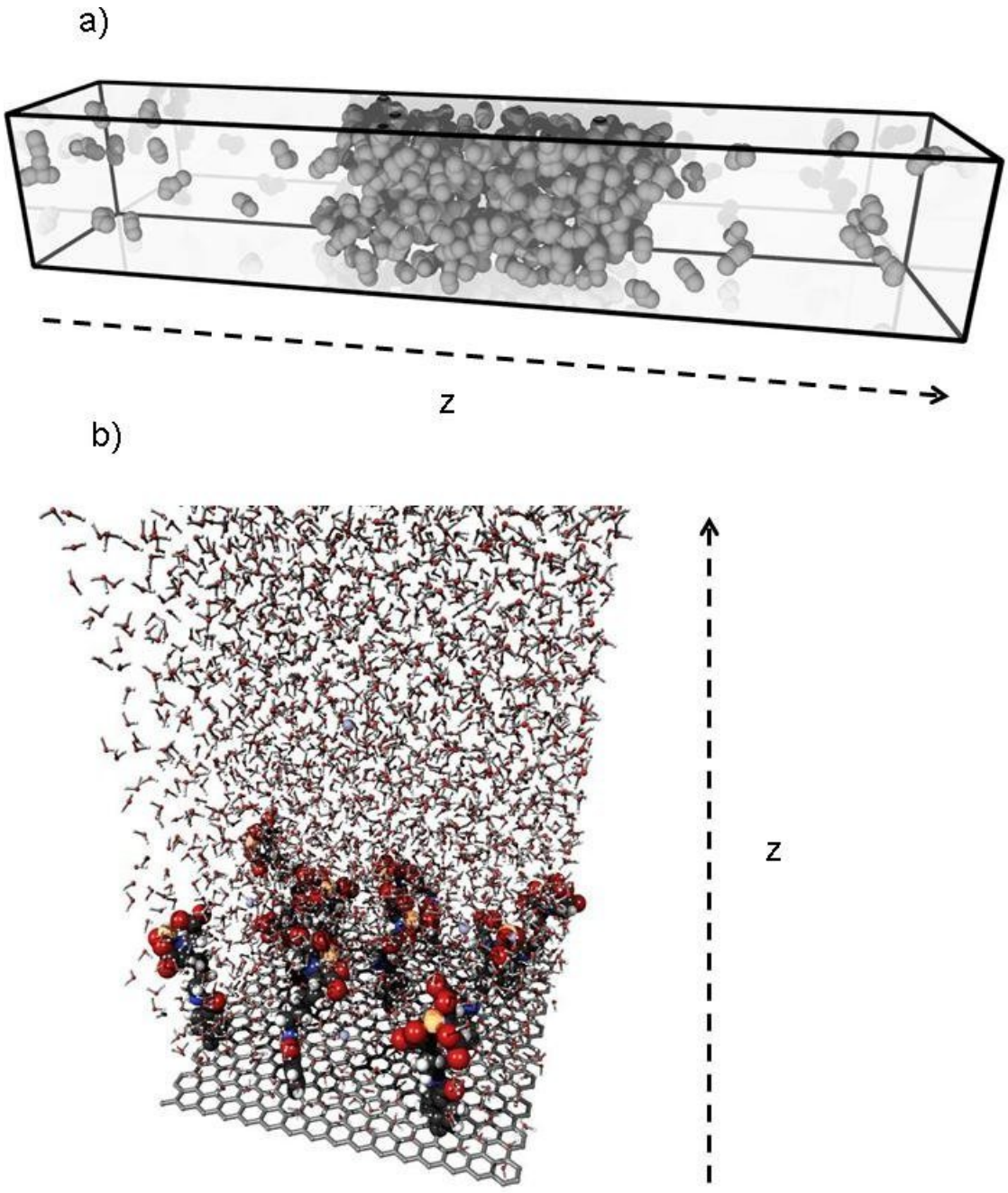

Figure 1:

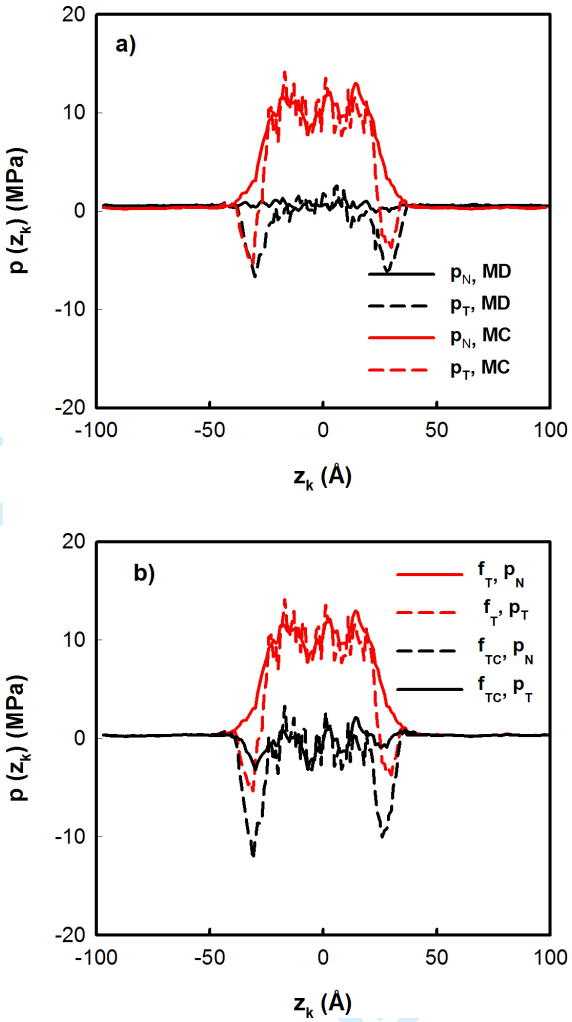

Figure 2:

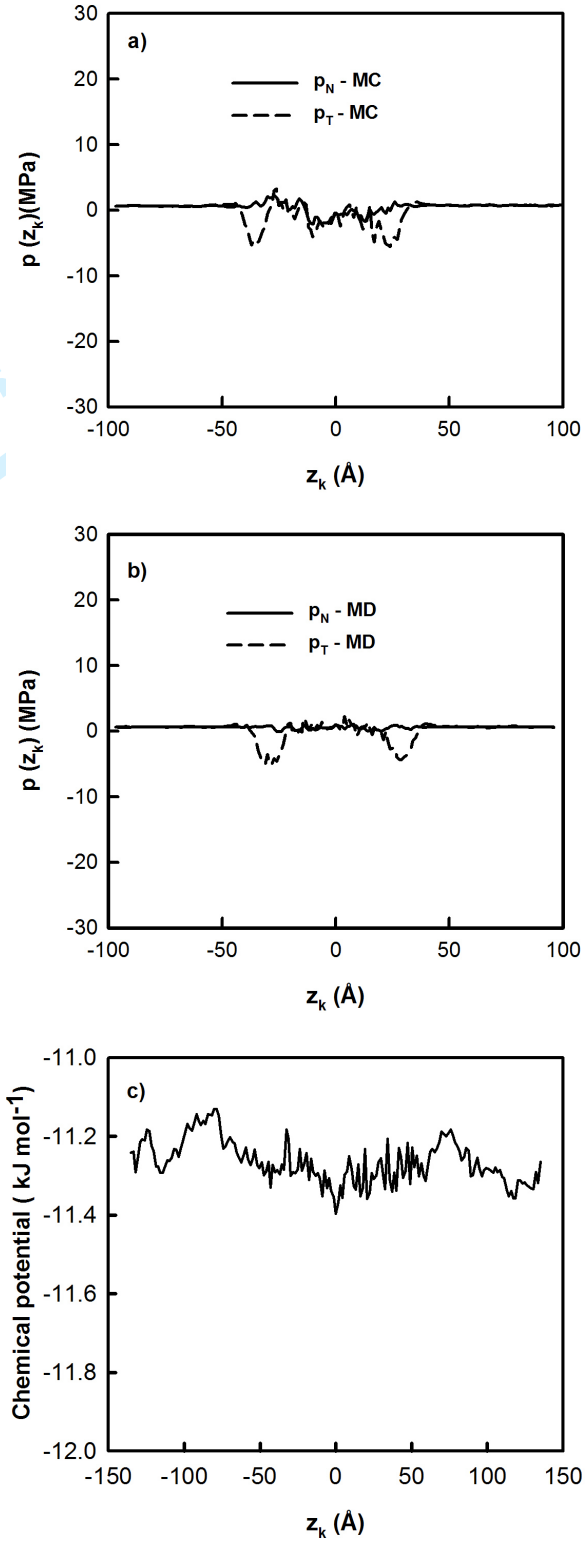
a)
p_N - MC
p_T - MC
p (z_k)(MPa)
z_k (Å)
b)
p_N - MD
p_T - MD
p (z_k) (MPa)
z_k (Å)
c)
Chemical potential (kJ mol^{-1})
z_k (Å)

Figure 3:

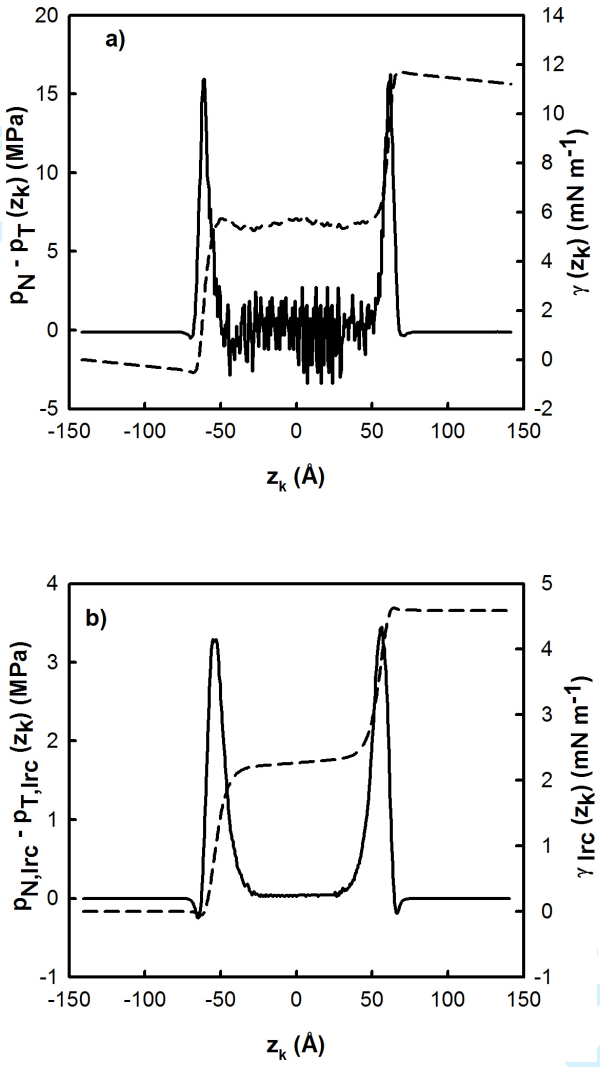
a)
$p_N - p_T (z_k)$ (MPa)
$\gamma (z_k)$ (mN m^{-1})
z_k (Å)
b)
$p_{N,Irc} - p_{T,Irc} (z_k)$ (MPa)
$\gamma_{Irc} (z_k)$ (mN m^{-1})
z_k (Å)

Figure 4:

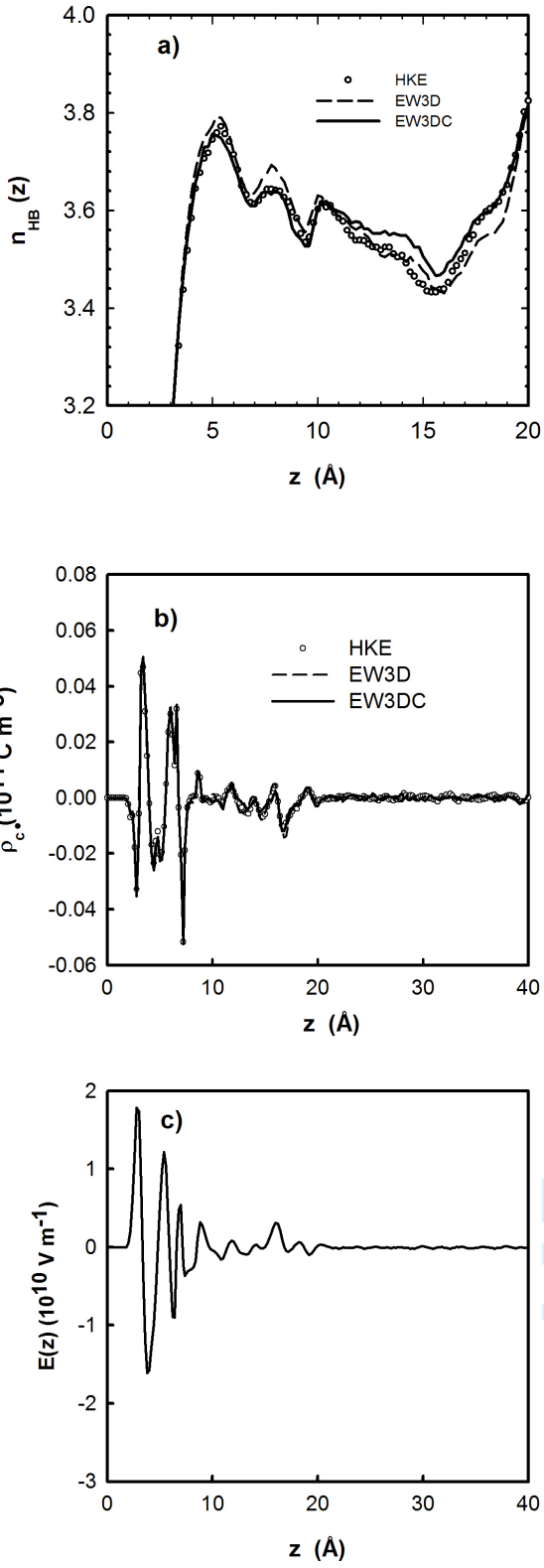
a)
HKE
EW3D
EW3DC
n_{HB} (z)
z (Å)
b)
HKE
EW3D
EW3DC
ρ_c.(10^{11} C m^{-3})
z (Å)
c)
E(z) (10^{10} V m^{-1})
z (Å)

Figure 5: